Silver Nanoplates: From Biological to Biomimetic Synthesis

Jianping Xie,[†] Jim Yang Lee,[†,§,*] Daniel I. C. Wang,[†,‡] and Yen Peng Ting[§]

[†]Singapore—MIT Alliance, 4 Engineering Drive 3, National University of Singapore, Singapore 117576, [‡]Department of Chemical Engineering, Massachusetts Institute of Technology, 77 Massachusetts Avenue, Cambridge, Massachusetts 02139, and [§]Department of Chemical and Biomolecular Engineering, National University of Singapore, 10 Kent Ridge Crescent, Singapore 119260

ABSTRACT This paper describes the synthesis of single-crystalline Ag nanoplates using the extract of unicellular green alga *Chlorella vulgaris* at room temperature. Proteins in the extract were involved in the biological synthesis, providing the dual function of Ag ion reduction and shape-controlled synthesis of nanosilver. Hydroxyl groups in Tyr residues and carboxyl groups in Asp and/or Glu residues were further identified as the most active functional groups for Ag ion reduction and for directing the anisotropic growth of Ag nanoplates, respectively. The kinetics of Ag ion reduction in biological systems was discussed and probed by using custom-designed peptides. The results showed the Tyr content (the reduction source) and the content of Ag complexers (the reaction inhibitors, *e.g.*, His and Cys) in the protein molecules as important factors affecting the reduction kinetics. The comprehensive system identification effort has led to the design of a simple bifunctional tripeptide (DDY-OMe) with one Tyr residue as the reduction source and two carboxyl groups in the Asp residues as shape-directors, which could produce small Ag nanoplates with low polydispersivity in good yield (>55%). The roles of the carboxyl groups in the formation of Ag nanoplates were also discussed.

KEYWORDS: biosynthesis · silver · proteins · biomimetic · peptides · nanomaterials

There has been increasing interest in the development of clean synthetic procedures ("green chemistry")[1] for nanoproducts targeted at biomedical applications. An environmentally acceptable solvent system and eco-friendly reducing and capping agents are three essential elements for a completely "green" nanoparticle synthesis. The biological approach to materials synthesis is ideal in this respect. In the past few years, numerous microorganisms have been applied to synthesize inorganic nanostructures either intracellularly or extracellularly. There are known bacteria for the production of metals (Ag[2,3] and Au[4,5]), sulfides (CdS[6] and ZnS[7]), and magnetite (Fe_3O_4[8]); yeasts for sulfides (PbS[9] and CdS[10]) and metal (Ag[11]); and fungi for metals (Ag[12,13] and Au[14]). While the formation of sulfides and magnetite by microorganisms has been understood to some extent, the synthesis of noble metal nanoparticles by microorganisms is a relatively recent discovery which is not well understood.

The surface plasmon properties of Ag nanomaterials are the foundation of a number of optics-based analytical techniques.[15–19] The biomedical applications of Ag nanoparticles have also attracted increasing interest,[20] such as employing the antimicrobial properties of Ag nanoparticles for wound healing.[21] While a number of biological species have been found to be capable of synthesizing Ag nanomaterials, the controllability of size and shape and the understanding of the principles involved are far from satisfactory. In the landmark work of Klaus *et al.*,[2] a metal-accumulating bacterium (*Pseudomonas stutzeri* AG259) was used as a "living factory" to generate, intracellularly, Ag-containing nanocrystals of different compositions (metallic Ag, monoclinic Ag sulfide (Ag_2S), and an undetermined structure) and morphologies (spherical, truncated triangular, triangular, and irregular shapes) with sizes ranging from a few nanometers to 200 nm. The defensive mechanism of the cell for Ag detoxification has been suggested as the biological pathway that reduced the Ag ions and precipitated the Ag compounds in the periplasmic space. Recently, several microorganisms normally not acclimatized to high concentrations of Ag ions, including bacteria[3] and fungi,[12,13] were also used to grow Ag nanoparticles intracellularly or extracellularly. In addition, several plant leaf extracts could also do the same.[22,23] As is common to current investigations on biological synthesis, most works have stopped at the phenomenological level without identifying the biomolecules involved in the synthesis of nanosilver. In the case of *Fusarium oxysporum*, Ahmad *et al.*[13] postulated, but without experimental evidence, an enzymatic process involving

*Address correspondence to cheleejy@nus.edu.sg.

Received for review July 5, 2007 and accepted November 26, 2007.

Published online December 28, 2007.
10.1021/nn7000883 CCC: $37.00

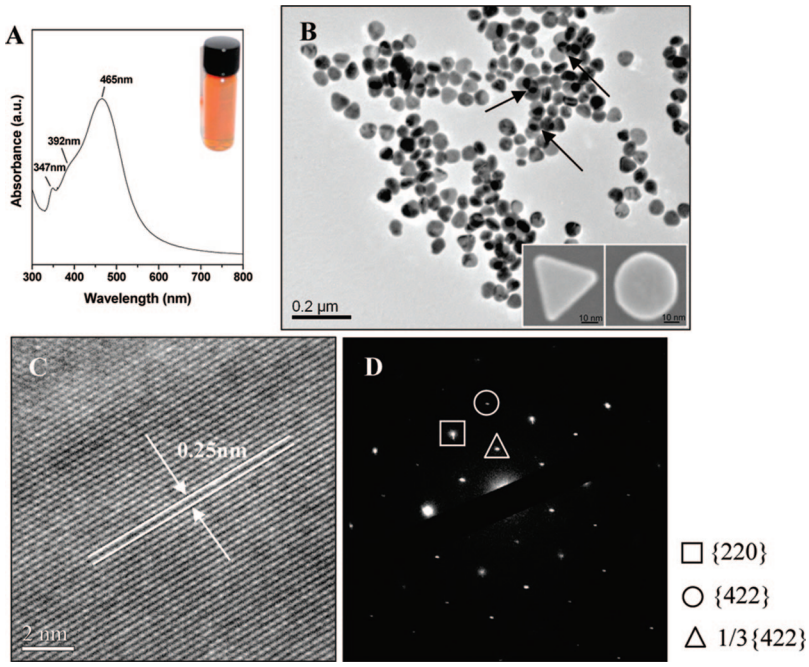

Figure 1. (A) UV–vis spectrum of Ag nanocrystals synthesized by reduction of aqueous Ag ion solution with the algal extract. The inset shows a digital image of the as-prepared Ag colloidal solution. (B) Representative TEM image of the as-prepared Ag nanocrystals. The arrows point to locations where several flat particles had overlapped. The inset shows typical FESEM images of circular and triangular Ag nanocrystals with a planar structure. (C) HRTEM image from the vertex of an isolated Ag nanoplate. (D) SAED pattern of a Ag nanoplate. The spots shown in a box, a circle, and a triangle correspond to {220}, {422} and 1/3{422} reflections, respectively.

certain NADH-dependent reductase for Ag nanoparticle synthesis. In a previous publication,[24] we reported the synthesis of Au nanoplates using the extract of unicellular green alga *Chlorella vulgaris* as reducing *cum* shape-directing agents. The results indicated the involvement of protein molecules. However, the biochemistry of the proteins in relation to the mechanisms of metal ion reduction and metal nanoplate formation was not understood because of the lack of experimental evidence.

This follow-up work made use of the extract of *C. vulgaris* to synthesize Ag nanomaterials, where Ag nanoplates were again formed as the principal product. Ag nanoplates have in the past been produced almost exclusively by photochemistry[25–28] and solution chemistry techniques.[29–32] The only known biological synthesis of Ag nanoplates made use of the bacterium *Pseudomonas stutzeri*.[2] The nanoplates were formed intracellularly with low yield and high polydispersity. Processing considerations generally do not favor the intracellular production of Ag nanoparticles because the product recovery steps would be cumbersome and expensive. The methodology presented here could be an inviting alternative by comparison. A simple, one-pot biological synthesis of large quantities of Ag nanoplates was accomplished by the room-temperature reduction of Ag ions in an aqueous algal extract. The kinetics of silver ion reduction and silver nanoplate formation were more amenable to analysis, allowing the roles of various functional amino acid residues in the biological synthesis to be better elucidated. It was found that the Tyr residues were the source of bioreduction and the carboxyl groups in Asp and/or Glu were primarily responsible for the anisotropic growth of the Ag nanocrystals. The major factors that affected the kinetics of Ag ion reduction were discussed and verified by using tripeptides containing different active residues. Finally, a custom-designed simple tripeptide was used as a proof of concept for the biomimetic synthesis of Ag nanoplates and to further test the particle formation mechanism. The information provided in this study can potentially bridge the divide between biological synthesis and biomimetic synthesis of Ag nanomaterials and motivate further work on the biomimetic synthesis of other noble metals. Presented below are the details of this investigation.

RESULTS AND DISCUSSION

Synthesis of Ag Nanoplates in Algal Extract. The algal extract was a light-yellow liquid. After it was contacted with 1 mM silver nitrate ($AgNO_3$) solution for 12 h at room temperature, the color changed to pinkish red (see the digital image in the inset of Figure 1A). The color change was caused by the surface plasmon resonance (SPR) of Ag nanocrystals in the visible region. Ag nanocrystals are known to exhibit size- and shape-dependent SPR bands[33–35] which can be characterized by UV–vis spectroscopy. We detected three plasmon bands located at *ca.* 465, 392, and 347 nm for the as-synthesized Ag nanocrystals (Figure 1A).

The as-synthesized Ag nanocrystals were analyzed by transmission electron microscopy (TEM) and electron diffraction. A typical TEM image (Figure 1B) reveals the presence of circular, rod-like, and triangular Ag nanocrystals. The triangular particles and some of the circular particles had uniform contrast, suggesting that they could be single-crystalline nanoplates. The plate-like morphology was confirmed by field emission scanning electron microscopy (FESEM) imaging of these particles (inset of Figure 1B), which showed that the rod-like particles were actually Ag nanoplates standing perpendicularly on the TEM grid. Also, at places where several planar particles overlapped (see arrows in Figure 1B), a darker region was produced. The distribution of circumscribed diameters from counting 100 Ag nanoplates yielded a mean of 44 nm and a standard deviation of 6 nm. The average thickness of the Ag nanoplates, estimated by measuring the width of the rod-like particles, was 20 ± 4 nm. Figure 1C shows a magnified high-resolution (HR) TEM image of the vertex of an isolated Ag nanoplate. The well-resolved inter-

ference fringe patterns attest to the single-crystallinity of the plate. The fringes were separated by 0.25 nm, usually assigned to forbidden 1/3{422} reflections, and justified as 3×{422} lattice spacing of the face-centered cubic (fcc) Ag crystal.[36–38] The single-crystallinity of these nanoplates was also confirmed by electron diffraction patterns (Figure 1D) obtained by aligning the electron beam normal to the planar surface. The six-fold symmetry of the diffraction spots indicates that the surface was bound by {111} faces. Three sets of spots could be identified on the basis of their *d*-spacings: the innermost set of spots with *d*-spacing of 0.25 nm was generated by the 1/3{422} reflection; the intermediate set of spots with the strongest intensity and *d*-spacing of 0.14 nm could be indexed to the {220} planes; and the outermost set with the weakest intensity and *d*-spacing of 0.08 nm was due to reflection from the {422} planes. These observations are consistent with previous findings on Ag or Au nanocrystals bounded by atomically flat surfaces.[25–32]

The presence of Ag nanoplates explains the observation of multiple SPR bands (465, 392, and 347 nm). According to the theoretical calculations by Jin *et al.*,[25] the multiplicity was caused by the in-plane dipole, out-of-plane dipole, and quadruple plasmon resonances of Ag nanoplates, respectively. The UV–vis spectrum (Figure 1A) of the algal-synthesized Ag nanoplates is also congruent with the optical extinction of Ag nanodisks previously reported by Chen *et al.*,[30] where absorptions at 475, ~420, and 351 nm were found for Ag nanodisks with diameter of ~60 nm and thickness of *ca.* 20–30 nm.

Identification of Components in the Algal Extract Active for Ag Nanoplate Formation. The reduction of Ag ions and the resulting growth of Ag(0) into Ag nanoplates must have been driven by some active species in the algal extract. In our previous work[24] we have identified proteins as the biomolecules involved in the morphosynthesis of gold nanoplates from chloroaurate ions. In this study, the algal proteins (*aP*) separated from the algal extract were again found to be primarily responsible for the reduction of Ag(I) and the formation of Ag nanoplates. Chemical modifications of *aP* were carried out to identify the amino acid residues in the proteins with Ag ion reduction capability and shape-directing functionality. A summary of the product morphology, product dimensions, SPR characteristics, and percentage conversions of Ag ions in different protein solutions is given in Table 1, from which the following conclusions may be made: (i) algal proteins were the active biomolecules in the algal extract for Ag nanoplate formation; (ii) Tyr residues in the proteins were responsible for Ag ion reduction; and (iii) the carboxyl groups in Asp and/or Glu residues were driving the anisotropic growth of Ag nanocrystals into nanoplates.

Proteins in the Algal Extract. The presence of proteins in the algal extract was confirmed by UV–vis spectroscopy and SDS−PAGE (Figure S1). The latter analysis also showed molecular weights in the range of 10–50 kDa. The proteins in the algal extract were first separated by dialysis according to size. The raw algal extract was divided into a low-molecular-weight fraction (MW < 7 kDa) and a high-molecular-weight fraction (MW ≥ 7 kDa, referred to as the algal proteins or *aP*) using a membrane tubing with molecular weight cutoff of 7 kDa. Each fraction was then individually tested for reaction with Ag ions in aqueous solutions. The UV–vis spectrum recorded for a 1 mM $AgNO_3$ aqueous solution after 12 h of reaction with the low MW fraction showed no absorption in the 300–800 nm region (curve 1, Figure 2A), whereas the high MW fraction (*aP*) produced a notable increase in absorption in the same period of time (curve 2, Figure 2A), due to the SPR of the Ag nanocrystals formed. Three absorption bands centered at *ca.* 500, 392, and 347 nm were clearly visible, indicating the formation of two-dimensional planar structures.

TABLE 1. Summary of Product Morphology, Product Dimensions, SPR Bands, and Percentage Conversions of Ag Ions in Different Reaction Media

reaction medium RM)[a]		product morphology and dimensions[b]	SPR bands (nm)	conversions, $[Ag(0)]/[Ag(I)]_{initial}$ (%)[c]
algal extract		nanodisks (~60%), av size ~44 nm	465, 392, 347	100
fractionated algal extract	low MW fraction (<7 kDa)	no product	n/a	0
	high MW fraction (≥7 kDa, *aP*)	truncated triangular plates (~80%), av size ~48 nm	500, 392, 347	98
modified algal proteins (*aP*)	heat-denatured	truncated triangular plates (~60%), av size ~27 nm	462, 393, 347	99
	urea-denatured	truncated triangular plates (~60%), av size ~26 nm	453, 390, 347	98
	NAI-modified	no product	n/a	0
	deacetylated NAI-modified	truncated triangular plates (~60%), av size ~46 nm	495, 388, 347	90
	amine-modified	irregular particles, av size ~29 nm	425	99

[a]The reaction mixture was prepared by adding 1 mL of 10 mM $AgNO_3$ to 9 mL of RM, and adjusting the pH to 7.0. [b]The dimensions of nanodisks and truncated triangular plates were measured by the circumscribed diameter and the longest edge of the truncated triangular plates, respectively. For all shapes, the dimensions were values averaged from over ~100 particles. [c]The percentage conversions of $AgNO_3$ to Ag were determined by atomic emission spectroscopy (AES) using an inductively coupled plasma (ICP) source.

The Ag nanocrystals formed in the *aP* solution were analyzed by TEM (Figure 2B). About 80% of them were truncated triangular plates (the rod-like particles and the truncated triangles were counted together), and the remaining ~20% were irregularly shaped. The average edge length and the thickness of the truncated triangular nanoplates were ~48 nm and ~21 nm (estimated from the widths of the rod-like particles), respectively. It should be mentioned that the shape of the nanoplates formed in the *aP* solution (truncated triangular) was different from the shape of the nanoplates formed in the algal extract (circular). The circular nanoplates (nanodisks)

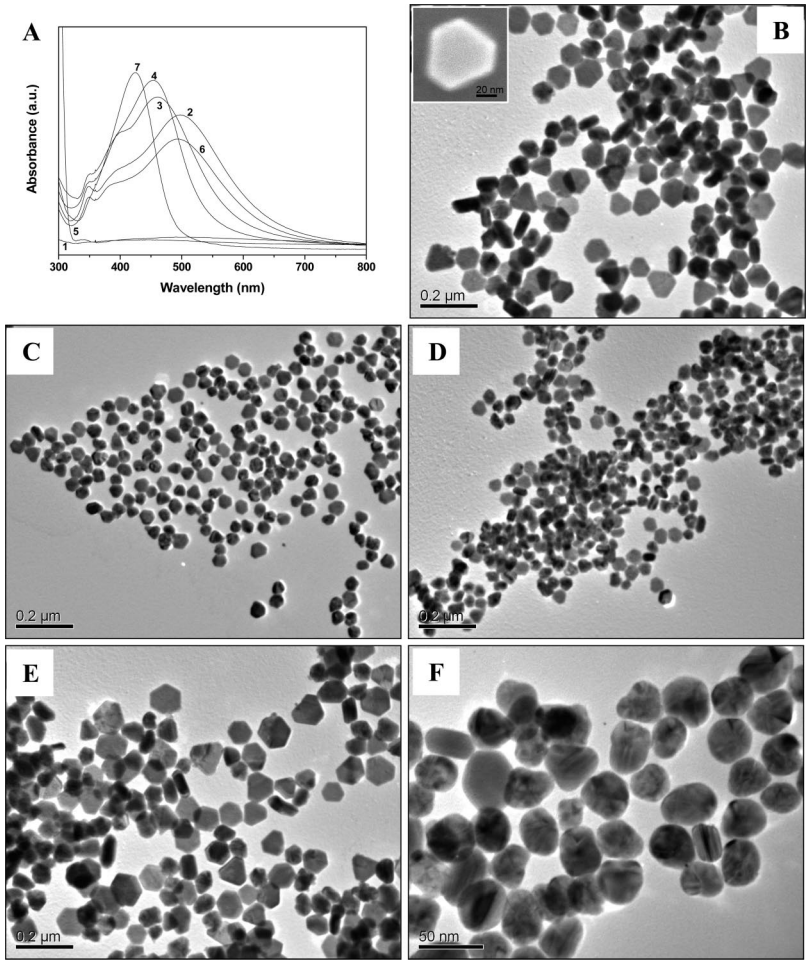

Figure 2. (A) UV–vis spectra of Ag nanocrystals obtained under different reaction conditions. Curves 1–7 were obtained by adding 1 mL of 10 mM $AgNO_3$ to 9 mL of (curve 1) low MW fraction of the algal extract; (curve 2) high MW fraction of the algal extract (*aP*); (curve 3) heat-denatured *aP*; (curve 4) urea-denatured *aP*; (curve 5) NAI-modified *aP*; (curve 6) deacetylated NAI-modified *aP*; and (curve 7) amine-modified *aP*, respectively. The pH of all solutions was adjusted to 7.0. (B–F) Representative TEM images of Ag nanocrystals prepared under conditions described in curves 2, 3, 4, 6, and 7, respectively. The inset in (B) shows a typical FESEM image of the truncated triangular plate, indicating the planarity of structure. All samples were collected at $t = 12$ h into the reaction.

The spectrum of the truncated triangular nanoplates (curve 2, Figure 2A) shows three absorption peaks at *ca*. 500, 392, and 347 nm, which correlate well with the in-plane dipole, the out-of-plane dipole, and the quadruple plasmon resonance of Ag nanoplates, respectively.[25] The red-shifting of the in-plane resonance (other SPR peaks were not as size-sensitive) from 465 nm (Figure 1A) to 500 nm was possibly caused by the larger aspect ratio of the truncated triangular nanoplates (edge length of ~48 nm) synthesized in the *aP* solution compared to the nanodisks (diameter of ~44 nm) formed in the raw algal extract.

Controlled experiments were then carried out to evaluate the effect of protein conformation on protein reactivity with the Ag ions. To achieve this, the heat-denatured and urea-denatured *aP* solutions were spiked with 1 mM $AgNO_3$ and allowed to stand for 12 h. The UV–vis spectra of the solutions after 12 h of reaction are shown as curves 3 and 4 in Figure 2A. The spectra are largely similar, displaying the characteristics of Ag SPR at *ca*. 462, 393, and 347 nm for the heat-denatured *aP* solution and at *ca*. 453, 390, and 347 nm for the urea-denatured *aP* solution. Figure 2C,D shows the corresponding TEM images of Ag nanocrystals formed in these solutions. The Ag nanocrystals had similar size and morphology, with truncated triangular nanoplates of edge length of ~27 nm as the main product (yield of ~60%). The blue-shifting of the in-plane SPR of Ag nanoplates (from 500 nm for pristine *aP* (curve 2, Figure 2A) to 462 or 453 nm for denatured *aP*) is consistent with the smaller aspect ratio of the nanoplates formed in these denatured protein solutions (27 *vs* 48 nm). Smaller nanoplates were formed because the unfolding of protein molecules upon denaturation significantly increased the accessibility of amino acid residues active in Ag ion reduction and in the growth-influencing selective adsorption of protein chains on specific Ag faces. The following hypotheses may be proposed on the basis of these observations. First, the reduction ability of protein(s) came directly from the amino residues rather than an enzyme-mediated process as was previously proposed for a fungal system.[13] Protein side groups, including amine, carboxyl, sulfhydryl, and hydroxyl moieties, were most likely the sites of action. Second, the soft-template mechanism generally proposed for surfactant-induced anisotropic growth of nanocrystals[41] could be ruled out here since the formation of the planar structure was achievable in pristine and denatured proteins which have very different conforma-

could be formed by the dissolution of the (more active) corner atoms of truncated triangular nanoplates. The selective dissolution process has been used by Chen *et al.*[30] to form Ag nanodisks from initial truncated triangular plates in the presence of Br^- ions, which were postulated as the etchant. More recently, Cl^- ion-assisted oxidative etching of Ag and Pd nanoparticles was also reported by Xia *et al.*[39,40] The presence of small molecular and/or ionic species in the algal extract, such as Cl^- ions, could have transformed the initially formed truncated triangular plates into nanodisks through a similar mechanism. However, small molecules were excluded from the *aP* solution, which had been dialyzed to retain only sufficiently large molecules, thereby allowing nanoplates with truncated triangular shapes to be formed as the stable final product. The effect of small molecules/ions on the shape transformation of Ag nanoplates is currently a working hypothesis.

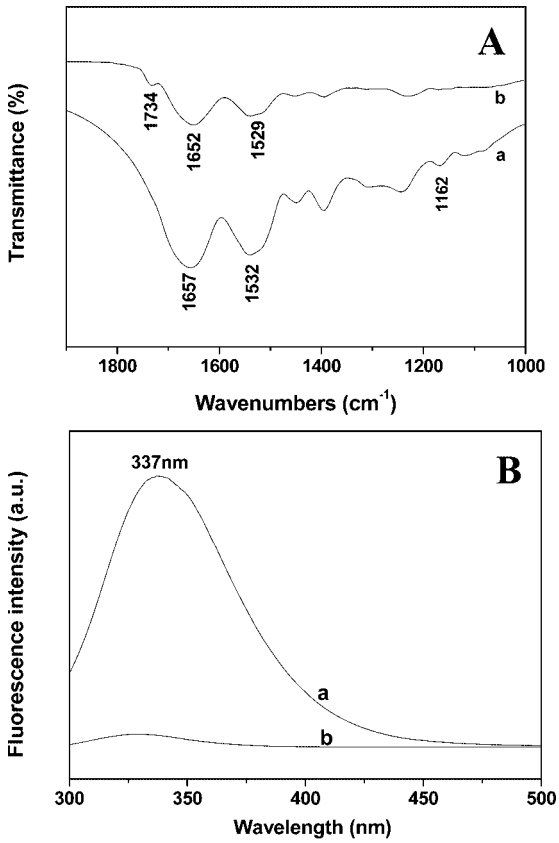

Figure 3. (A) FTIR and (B) fluorescence spectra of the algal proteins: (curve a) pristine algal proteins and (curve b) protein/Ag nanocrystal bioconjugates after 12 h of reaction.

tions. Thus, we believe that the formation of planar Ag nanostructures was initiated by the specific interaction of protein molecules with Ag ions and Ag surface, with the latter resulting in the anisotropic growth of Ag nanocrystals. The natural next order of experimentation was to determine the active amino residues in protein molecules for Ag ion reduction and for directing of anisotropic growth of Ag nanocrystals.

Tyrosine Residues and Ag Ion Reduction. The nature of the amino acid residues in the algal proteins for Ag ion reduction was first revealed by FTIR and fluorescence analyses of the protein structure before and after reaction with Ag ions, as shown in Figure 3. The 1657 and 1532 cm^{-1} peaks in the FTIR spectrum of freeze-dried pristine *aP* in KBr pellet (curve a of Figure 3A) are characteristic of the amide I and amide II bands of proteins. The peak at 1162 cm^{-1} due to the phenolic group of Tyr residues was conspicuously absent in the FTIR spectrum of *aP* after reaction with Ag ions (curve b of Figure 3A). The disappearance of the 1162 cm^{-1} peak, which may be taken as the depletion of the phenolic residues, was accompanied by the concomitant appearance of carbonyl stretching at 1734 cm^{-1}, traceable to the formation of a phenoxide structure from the oxidation of the Tyr phenolic group. The involvement of Tyr residues in the reduction of Ag ions was further confirmed by fluorescence analysis of Tyr signatures before (curve a, Figure 3B) and after (curve b, Figure 3B) Ag ion reduction. The intrinsic fluorescence of Tyr is sensitive to oxidation,[42] and the loss of fluorescence indicates the oxidation of the phenolic group of Tyr. As shown in Figure 3B, most, if not all, of the fluorescence of Tyr residues in the algal proteins was lost after reaction with Ag ions, indicating the nearly complete oxidation of the phenolic groups of the Tyr residues.

The involvement of Tyr residues in the reduction of Ag ions could be demonstrated more elegantly by using chemical modifications that switched on and off the Tyr functionality. Chemical modifications of specific amino acid residues have been commonly used to study the structure–function relationship of specific residues in a given protein. N-Acetylimidazole (NAI), first introduced by Riordan *et al.*,[43,44] is a mildly selective protein-acetylating reagent that preferentially acetylates exposed Tyr residues in neutral pH solution (reaction 4). However, it can also react with other amino acid residues containing the hydroxyl group, such as serine and threonine.

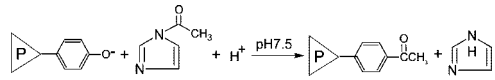

(1)

In order to ensure that all Tyr residues would be acetylated, the algal proteins were acetylated in the presence of the denaturant (8 M urea), which unfolded the proteins.[43,44] The UV–vis spectrum of 1 mM aqueous solution of $AgNO_3$ after 12 h of reaction with the NAI-modified *aP* showed no absorption in the 300–800 nm region (curve 5, Figure 2A). The lack of reactivity was an indication of the loss of Tyr participation in the Ag ion reduction reaction and contrasted strongly with the case of Ag nanocrystal formation in denatured *aP* solution before NAI acetylation (curve 4, Figure 2A). The involvement of the tyrosyl hydroxyl groups in Ag ion reduction was also confirmed by a comparative study using L-tyrosine and *O*-methyl-L-tyrosine, where the methylation of the hydroxyl group led to the complete loss of reduction capability for Ag ions (see Figure S2 in the Supporting Information for the UV–vis spectra of the two reaction mixtures after 8 h of reaction). The specificity of the Tyr involvement in Ag ion reduction reaction was proved by the deacetylation of NAI-modified *aP*. It is well-known that hydroxylamine deacetylates acetyl-tyrosine to regenerate the hydroxyl functional group at pH 7.5, but not acetyl-serine or acetyl-threonine.[45] Accordingly, the hydroxylamine treatment is a specific procedure effective only for the reactivation of NAI-modified Tyr residues. The UV–vis spectrum recorded for a 1 mM $AgNO_3$ aqueous solution after 12 h of reaction with the deacetylated NAI-modified *aP* was similar (curve 6, Figure 2A) to the absorption spectrum of Ag nanocrystals synthesized in the pristine *aP* solution (curve 2, Figure 1A), thereby providing unequivo-

cal proof that the Tyr residues were involved in the reduction of Ag ions. The Ag nanocrystals prepared with deacetylated NAI-modified *aP* were analyzed by TEM. As shown in Figure 2E, truncated triangular nanoplates with average edge length of ~46 nm were produced in ~60% yield.

Carboxyl Groups in Asp and/or Glu Residues and the Anisotropic Growth of Ag Nanoplates. Strong signature carboxyl absorption (1405 cm^{-1})[46] was detected in the FTIR spectrum of the algal proteins (spectrum a, Figure 3A). The carboxyl groups in the amino acid residues were found to promote the anisotropic growth of nanoparticles into nanoplates. This could be easily demonstrated through the amination modification of the residues, which converted all of the carboxyl groups in Asp and/or Glu into amine groups.[47] The UV–vis spectrum of a 1 mM $AgNO_3$ solution after 12 h of reaction with amine-modified *aP* showed only one absorption peak at ~425 nm (curve 7, Figure 2A), which is typical of spherical Ag nanoparticles. The preponderance of spherical Ag nanoparticles in the product was confirmed by TEM (Figure 2F), which also showed some irregularly shaped structures with no regular anisotropy, besides the spherical particles. It is therefore reasonable to deduce that the carboxyl groups in Asp and/or Glu residues possess shape-directing functionality; without them, isotropic growth of nanocrystals would prevail, leading to mostly spherical Ag nanoparticles.

The involvement of Tyr residues in the reduction of Ag ions could also find supporting evidence from previous studies.[48,49] Naik *et al.*[48] identified three Ag-binding peptides (dodecapeptides AG3, AG4, and AG5) by combinatorial approaches using a phage display peptide library. The AG3 and AG4 peptides were active for the reduction of Ag ions to Ag nanoparticles. A mixture of shapes (spheres and hexagonal and triangular plates) was obtained. Interestingly, the AG3 (A<u>Y</u>SSGAPPMPPF) and AG4 (NPSSLFR<u>Y</u>LPSD)) peptides also contain the Tyr residue implicated here to be responsible for Ag ion reduction. In contrast, the Ag-binding peptide without the Tyr residue (AG5 (SLATQPPRTPPV)) could not reduce Ag ions. The presence of an Asp residue in AG4, which formed nonspherical (hexagonally and triangularly shaped) Ag nanocrystals, also correlated with the shape-directing functionality of the carboxyl groups in Asp and/or Glu residues discovered here.

Roles of Amino Acid Residues in the Biological Synthesis of Ag Nanomaterials. ***Kinetic Factors in Ag Ion Reduction.*** Algal proteins were therefore multifunctional agents capable of reducing Ag ions in aqueous solution to Ag(0) and directing the embryonic Ag clusters to grow anisotropically into nanoplates with {111} planes on their open faces. The hydroxyl groups in the Tyr residues were active for Ag ion reduction, and the carboxyl groups in Asp and/or Glu residues were responsible for inducing the anisotropic growth of Ag nanocrystals. Works in the past decade have found a large number of biological species,

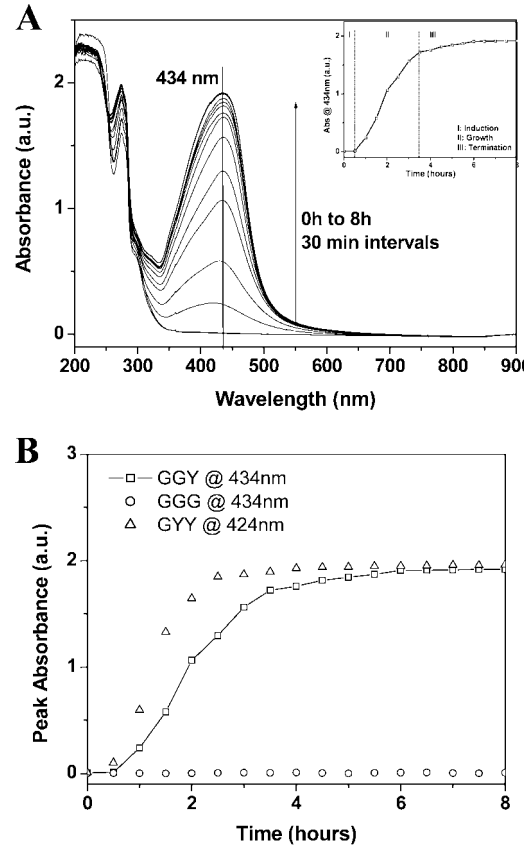

Figure 4. (A) Time-resolved UV–vis spectra of reaction solution of $AgNO_3$ with GGY at room temperature. The spectra were recorded every 30 min. The inset shows the corresponding time course plot of absorption intensity at 434 nm, indicating a characteristic sigmoidal shape of three distinct reaction phases. (B) Time course plots of absorption intensity at typical Ag SPR frequencies for GGY, GGG, and GYY. The pH of all reaction mixtures was adjusted to 9.0.

including bacteria,[3,4] fungi,[12,13] yeasts,[11] and plant leaves,[22,23] active for the reduction of Ag ions to Ag nanocrystals. The findings in this study provide a basis for understanding the biological activities by identifying Tyr residues as an important and common (if not the only) reduction source in these systems. Differences in the composition of protein side groups, especially the Tyr content, may account for the different activities displayed by the different biological systems. Biological systems that are more reactive with Ag ions may be richer in Tyr residues or have Tyr residues that are less sterically hindered for reaction. This hypothesis was verified by reacting Ag ions with three custom-designed tripeptides containing different numbers of Tyr residues (GGG, GGY, and GYY). GYY was found to be more active than GGY, and GGG showed no apparent reactivity in Ag ion reduction. Figure 4A shows the time-resolved UV–vis spectra of the reaction between $AgNO_3$ and GGY at pH 9.0, and the inset shows the corresponding absorption at 434 nm (Ag SPR) as a function of time. The time course showed a characteristic sigmoidal shape consisting of three distinguishable reaction regimes: (I) a short induction period lasting ~0.5 h, (II)

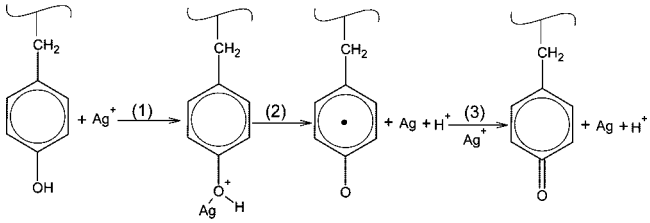

Figure 5. Reactions of Ag ions with a Tyr residue. Two Ag ions are reduced to elemental Ag, and two protons are generated.

a rapid growth phase between ~0.5 and 3.5 h, and (III) a plateau signaling the end of reaction. The plots of absorbance with time at typical Ag SPR frequencies for GGY, GGG, and GYY are given in Figure 4B.

Our results implicating the involvement of the Tyr hydroxyl group in Ag ion reduction also find supporting evidence in the biological systems. It has been reported that tyrosine plays an important role in electron transfer in the photosystem II (PSII) of photosynthesis,[50] where a neutral tyrosyl radical is generated. The pH dependence of the rate constant for electron transfer from Tyr in the PSII system has been investigated by Sjodin *et al.*,[50] where proton-coupled electron transfer was proposed for pH $<$ 10 (below the Tyr pK_a $\approx$ 10) and single-electron transfer was proposed for pH $>$ 10 (above the Tyr pK_a). Since the reactions in this study were carried out at pH $<$ 10, the Tyr groups were initially protonated, and a similar proton-coupled electron-transfer mechanism could also be at work for the reduction of Ag ions, as schematized in Figure 5. The first step of this mechanism involves a Ag ion acting as Lewis acid to bind with the lone pair of electrons on the Tyr oxygen. The Ag ion then picked up an electron from Tyr to become elemental Ag, which was released with the concomitant deprotonation of Tyr in a single, concerted step (step 2). The Tyr cation was stabilized by the delocalization of free electrons in the π system of the ring. The oxygen on the tyrosyl radical was open to attack by a second Ag ion. As the second Ag ion was reduced together with the release of a second proton, a stable quinoid structure was formed (step 3).

It is also important to consider the possibility of Ag ion complexation in reduction. Ag ions are known to complex with the following side groups in the amino acid residues: Asp, Glu, His, Cys, Lys, and Met.[51,52] The driving force for Ag nanocrystal synthesis in protein solutions came from the following simple redox reaction, where a Ag ion was reduced by accepting an electron from a Tyr residue, which became oxidized in the process.

$$Ag^+ + e^- \rightarrow Ag$$

$$\text{p-Tyr-OH} \rightarrow \text{p-Tyr}{=}\text{O} + 2H^+ + 2e^-$$

The standard electrode potential of Ag^+/Ag redox is 0.8 V.[53] However, this value can be significantly different when the Ag ions are complexed. Generally, complexation lowers the redox potential and hence the reducibility of Ag ions. Examples include Ag halides used for photography (AgBr, 0.07 V), Ag diamine complexes ($Ag(NH_3)_2^+$, 0.37 V), and complexes formed in an alkaline medium (Ag_2CO_3, 0.47 V; AgOH, 0.24 V). This could also be understood as the need for the complex to dissociate into free Ag ions before reduction occurs.

When Ag ions were incubated with a protein solution, the Ag ions could be present in two forms: (a) free in solution and (b) strongly bound to proteins by way of salt formation with the $-COO^-$ groups (Asp and Glu) or by complex formation with the nucleophilic groups in the residues, such as imidazole (His), $-SH$ (Cys), $-SCH_3$ (Met), and $-NH_2$ (Lys). The reducibility of the Ag complex should decrease with increasing binding strength. Several custom-designed tripeptides (X-X-Tyr-OMe) were used to illustrate this point. Three types of residues were used for X: (a) X = Gly to represent nonfunctional side groups; (b) X = Ser to represent hydroxyl side groups; and (c) X = His, Cys, Lys, and Asp to represent four different types of complexing side groups. From the plots of absorbance at prevailing Ag SPR frequencies *versus* time shown in Figure 6, the following reactivity order was obtained: SSY $\approx$ GGY $>$ KKY $>$ DDY. No reaction occurred for CCY and HHY within the same period of time (8 h). No distinctive difference was found between SSY and GGY, which indicates negligible complexing ability of the hydroxyl groups in Ser residues. In CCY and HHY, most of the Ag ions are believed to be bound strongly at the imidazole (His) or thiol (Cys) sites, preventing spontaneous reaction, resulting in no apparent reactivity in the same period of time (8 h). In the KKY and DDY systems, the binding of the Ag ions at the amine (Lys) or carboxylic (Asp) sites was weaker than in the case of binding with the imidazole (His) or thiol (Cys) sites, and Ag ions could be reduced slowly by the peptides, albeit at a rate much slower than in the case of GGY and SSY.

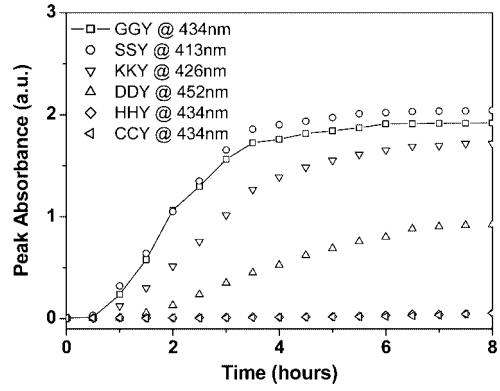

Figure 6. Time course plots of absorption intensity at typical Ag SPR frequencies for GGY, SSY, KKY, DDY, HHY, and CCY. The pH of all reaction mixtures was adjusted to 9.0.

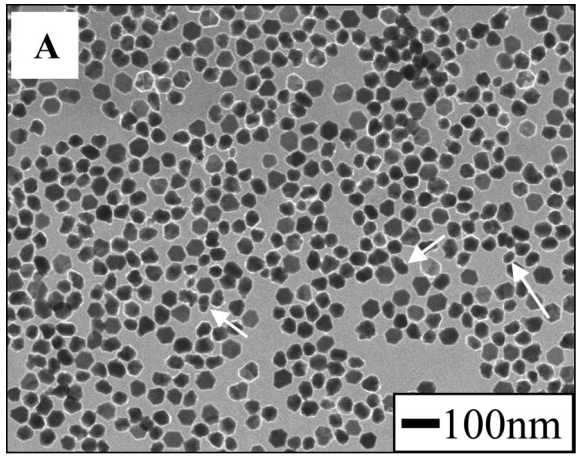

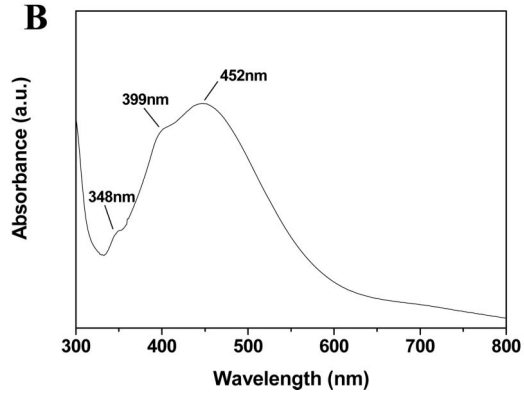

Figure 7. Representative FESEM image (A) and UV–vis spectrum (B) of Ag nanocrystals synthesized in DDY peptide solution. Arrows in (A) show truncated triangular Ag nanoplates standing perpendicularly on the TEM grid, resulting in a rod-like appearance.

Factors Affecting the Anisotropic Growth of Ag Nanocrystals. It is not yet possible to provide a detailed mechanism for the oriented growth of Ag nanocrystals in the *aP* solution since the biochemistry of *aP,* and the separation and purification of the active components in *aP*, still need extensive further work. Nevertheless, some guiding principles on peptide design to achieve shape-selective synthesis of Ag nanomaterials may be deduced from the experimental results presented here, so as to provide the necessary first step in the biomimetic shape-controlled synthesis of Ag nanomaterials. The finding that the carboxyl groups in Asp and/or Glu residues were involved in the anisotropic growth of Ag nanocrystals into nanoplates was used in the preliminary design of a bifunctional short peptide for the synthesis of Ag nanoplates. The simple tripeptide, DDY-OMe, was synthesized and tested with Ag ions. In this tripeptide the Tyr residue served as the electron source for Ag ion reduction and the two Asp residues played the role of shape-directing agents. Figure 7A shows a representative FESEM image of the as-synthesized Ag nanocrystals, where small truncated triangular and irregularly shaped Ag nanoparticles were found. As the truncated triangular nanoplates could have been imaged in all possible projections and hence showing various faceted structures, it was difficult to quantify the yield of the truncated triangular nanoplates accurately. Nevertheless, an estimated 55% yield was obtained by counting only the truncated triangles and rod-like particles together in the TEM image. The longest edge of the truncated triangular nanoplates averaged to 28.3 $\pm$ 3.1 nm. The average thickness, estimated from the width of the rod-like nanocrystals (highlighted by arrows in Figure 7A), was about 11.2 nm. It should be emphasized that the synthesis of small (*i.e.*, $<$30 nm) nanoplates is a current challenge, and most of the nanoplates synthesized to date and reported in the literature were larger than 50 nm.[25–32] This is perhaps the first successful attempt at the biomimetic synthesis of truncated triangular nanoplates smaller than 30 nm with low polydispersivity and good yield, which should improve the usability of the Ag nanoplates in bioimaging and as near-field optical probes.[33–35] The as-synthesized Ag nanoplates have SPR bands (*ca.* 452, 399, and 348 nm, Figure 7B) similar to the algal-synthesized Ag nanoplates (curve 2, Figure 2A). The synthesis of Ag nanoplates in DDY peptide solution corroborated the role of carboxyl groups in directing the formation of Ag nanoplates in the algal system.

While it is not clear at the molecular level how the carboxyl groups enacted the shape-controlled synthesis, there were several revealing experimental observations:

(i) The formation of Ag nanoplates in the algal protein or DDY solution was a kinetically controlled process. The molecular recognition properties of peptides for specific crystallographic planes and the slow-growth condition are two determining factors in the formation of planar Ag nanostructures. Experimentally, the flat open faces of the plate-like structures were all ⟨111⟩ oriented, suggesting the selective adsorption of growth-inhibiting species on the {111} planes. Truncated octahedron and multiple twinned particles (origin of spherical particles) are the thermodynamically favorable shapes for a fcc metal, and hence the reaction of Ag ions with the algal protein or DDY solution at 100 °C (very fast reaction) produced almost exclusively spherical particles (data not shown). Besides the face recognition ability of DDY molecules, the complexation of Ag ions or Ag intermediate reaction products to the carboxyl groups of DDY was also an advantage: the resulting slow-down of the reduction kinetics favored the formation of Ag nanoplates, as shown by the success of the DDY solution in synthesizing Ag nanoplates. The effect of Ag complexation to the carboxyl groups on particle growth has been reported by Pillai *et al.*,[54] using a tricarboxylic acid (citric acid). It was stated that one of the primary intermediates, Ag_2^+, could readily interact with the carboxyl groups of citrate to form a complex [Ag_2^+−citrate], which underwent slower transformations compared to uncomplexed Ag_2^+. In addition, there were also several reports implicating citrate as

the shape-directing agent in the formation of plate-like Ag or Au nanostructures.[26,27,55] Hence, the shape-directing capability of DDY, which contains two carboxyl groups per molecule, was not at all unexpected.

(ii) The ratio of carboxylic groups to Tyr per peptide molecule is an important consideration in the synthesis of Ag nanoplates with good yield. Comparative experiments were carried out using peptides without a carboxyl group (GGY-OMe, SSY-OMe, and KKY-OMe) and peptides with one (GDY-OMe) and four carboxylic groups per unit (poly(Glu, Tyr) (4:1, MW of 20–50 kDa)). Irregularly shaped and spherical Ag nanocrystals were the main products (with less than 5% of Ag nanoplates) in syntheses with peptides without a carboxyl group (GGY-OMe, SSY-OMe, and KKY-OMe). Ag nanoplates were obtained in low yield (~15%) in peptide with one carboxyl group (GDY-OMe), while Ag nanoplates were formed in good yield (~60%) using polypeptides with four carboxyl groups per unit (see Figure S3 for FESEM images and UV–vis spectra and Table S1 for a summary of product morphology, product dimensions, SPR characteristics, and percentage conversions of Ag ions).

On the basis of these observations, it is reasonable to conclude that the moderation of the Ag ion reduction kinetics by multiple carboxyl groups in proteins/peptides and the interactions of the carboxyl groups with Ag ions, Ag reaction intermediates, and Ag surface (molecular recognition of crystallographic planes) all contributed to the anisotropic growth of Ag nanocrystals into nanoplates in good yield. A computational study on the interaction of peptide (DDY-OMe) with Ag ions, Ag reaction intermediates, and Ag surface (nanocrystals facetted by {111} and {100} planes) is currently underway, which may help to provide further information.

CONCLUSIONS

A simple room-temperature one-pot synthesis based on the bioreduction ability of an algal extract solution has been developed to produce Ag nanoplates. Microstructural characterizations by TEM, HRTEM, and selected area electron diffraction showed that the nanoplates were oriented with {111} planes as the basal plane. The experimental results implicated proteins as the active biomolecules involved in the synthesis of Ag nanoplates. The hydroxyl groups in Tyr residues and the carboxyl groups in Asp and/or Glu residues were found to be responsible for Ag ion reduction and for the anisotropic growth of Ag nanocrystals into nanoplates, respectively. The kinetics of Ag ion reduction depended not only on the Tyr content (the electron source) but also on moieties such as His and Cys residues in the proteins which could complex well with the Ag ions (reaction inhibitors). The system identification effort resulted in the design of a simple bifunctional tripeptide (DDY) containing one Tyr residue and two Asp residues which was able to produce small Ag nanoplates in good yield (>55%) and with low polydispersivity. The formation of Ag nanoplates was found to be a kinetically controlled process, depending on the ratio of carboxyl groups to Tyr per peptide molecule, as a result of the interactions between carboxyl groups with Ag ions, Ag reaction intermediates, and Ag surface.

EXPERIMENTAL METHODS

All chemicals were purchased from Sigma-Aldrich and used as received. Custom-designed tripeptides were supplied by GenScript Corp. (Piscataway, NJ) and Sigma-Aldrich. Ultrapure Millipore water (18.2 MΩ) was used as the solvent throughout.

Preparation of Algal Extract. The unicellular green alga *Chlorella vulgaris* (Cambridge collection strain no. 211/11b) was batch cultured as described previously.[24] The algal cells after 10 days of culture were separated by centrifugation, washed with 1% HNO_3, rinsed with ultrapure water to remove adsorbed impurities, and lyophilized. Fifty milligrams of lyophilized algal cells was dispersed in 10 mL of ultrapure water. The supernatant (the algal extract) was separated from the biomass two days later by filtration through Whatman Autovials (0.45 μm).

Separation of Proteins in the Algal Extract. The raw algal extract (10 mL) was dialyzed in a membrane tubing with a molecular weight cutoff of 7 kDa against 1 L of continuously stirred ultrapure water at room temperature. Twenty-four hours and three water changes (at 8 h intervals) later, the tubing content (the high-molecular-weight components) was collected and labeled as the algal proteins, or *aP*. The optical density of the *aP* solution at 280 nm (OD_{280}) was 1.5, and this was used as an indirect measure of the protein concentration.

Modifications of *aP*. *Preparation of Denatured aP.* For the denaturation of the algal proteins, 10 mL of the pristine *aP* solution ($OD_{280} \approx 1.5$) was boiled for 30 min (heat-denatured *aP*) or mixed with 8 M urea solution and incubated for 3 h (urea-denatured *aP*). After the heat-treated solution was cooled to room temperature or the urea was dialyzed out from the urea-treated solution, ultrapure water was added to the denatured *aP* solution to a final volume of 10 mL, and the solution was stored at 4 °C until use.

Chemical Modifications of the Tyr Residues in aP with N-Acetylimidazole (NAI). NAI-modified *aP* was prepared according to the procedure of Zhang *et al.*[56] Briefly, an aqueous solution of NAI was prepared immediately before use. The acetylation of the Tyr residues in *aP* ($OD_{280} \approx 1.5$) was carried out in excess NAI solution and in the presence of the denaturant (8 M urea). Specifically, the algal proteins were incubated with 8 M urea for 1 h before a 50 mM NAI aqueous solution was added. The mixture was then incubated at 37 °C for 2 h and dialyzed against ultrapure water for 24 h to recover the NAI-modified *aP*.

Deacetylation of NAI-Modified aP by Hydroxylamine. For deacetylation, hydroxylamine was added to NAI-modified *aP* in a pH 7.5 phosphate buffer to a final concentration of 1 M. The mixture was then incubated at room temperature for 1 h and dialyzed against ultrapure water for 24 h to recover the deacetylated NAI-modified *aP*.

Amination of the Carboxyl Groups of aP. Amination of the carboxyl groups of *aP* was carried out using the urea-denatured *aP* solution and following the procedure of Lopez-Gallego *et al.*[47] In brief, 5 mL of urea-denatured *aP* ($OD_{280} \approx 1.5$) was added to 45 mlf 1 M ethylenediamine (EDA) at pH 4.75. Solid 1-ethyl-3-(3-dimethylaminopropyl)carbodiimide (EDAC) was added to the mixture to a final concentration of 10 mM. After 90 min of gentle stirring at 25 °C, 10 mL of 0.5 M hydroxylamine solution at pH 7 was introduced. The protein solution was then dialyzed against ultrapure water for 24 h to recover the amine-modified *aP*. It has been reported that the use of 1 M EDA at pH 4.75 and 10 mM

EDAC would allow the full amination of the carboxyl groups of proteins.[47]

Synthesis of Ag Nanoparticles. ***Synthesis of Ag Nanoplates Using Algal Extract.*** In a typical experiment, 1 mL of 10 mM $AgNO_3$ was added to 9 mL of algal extract, and the reaction was allowed to proceed under gentle stirring at room temperature for 12 h. The pH of the reaction medium was adjusted to 7.0 by adding 1 M NaOH solution.

Synthesis of Ag Nanoparticles Using Pristine and Modified aP. The syntheses of Ag nanoparticles by pristine and differently denatured and modified (heat-denatured, urea-denatured, NAI-modified, deacetylated NAI-modified, and amine-modified) *aP* were carried out under the same conditions as those used for the synthesis in algal extract, except for the substitution of the algal extract by the *aP* solution. The optical densities of all *aP* solutions at 280 nm were adjusted to a value of ~1.5.

Synthesis of Ag Nanoparticles Using Custom-Designed Tripeptides. C-terminal methylated tripeptides Gly-Gly-Gly-OMe (GGG), Gly-Gly-Tyr-OMe (GGY), Gly-Tyr-Tyr-OMe (GYY), Ser-Ser-Tyr-OMe (SSY), Lys-Lys-Tyr-OMe (KKY), Asp-Asp-Tyr-OMe (DDY), His-His-Tyr-OMe (HHY), and Cys-Cys-Tyr-OMe (CCY) were dissolved in ultrapure water and freshly prepared before use. In a typical experiment, 100 μL of 10 mM $AgNO_3$ was added to 1 mL of 2 mM tripeptide solution. The pH of the reaction mixture was adjusted to 9.0, and the reaction was carried out under gentle stirring at room temperature for 8 h.

Materials Characterizations. UV–vis spectroscopy was performed on a Shimadzu UV-2450 instrument operating at 1 nm resolution. Examinations of nanoparticle size and morphology made use of a JEOL JSM-6700F microscope operating at 25 kV (for FESEM imaging), a JEOL JEM-2010 microscope operating at 200 kV (for TEM imaging), and a JEOL JEM 2010FE microscope operating at 200 kV (for high-resolution TEM imaging). Fourier transform infrared spectroscopy (FTIR) was carried out on a Shimadzu FTIR-8400 spectrometer in the diffuse reflectance mode at a resolution of 4 cm^{-1}. Fluorescence emission spectra were measured with a Photon Technology International QuantaMaster system using an excitation wavelength of 280 nm. The percentage conversions of $AgNO_3$ to Ag were determined by atomic emission spectroscopy (AES). The AES measurements were carried out on a Perkin-Elmer Optima 3000DV atomic emission spectrometer using an inductively coupled plasma (ICP) source. Ag nanoparticles were collected by centrifugation after reaction and then dissolved in aqueous HNO_3 solution (60%). The emission at 328 nm was used to measure the concentration of the Ag atoms. The percentage conversion was calculated on the basis of the amount of dissolved Ag atoms in the HNO_3 solution and the amount of $AgNO_3$ present in the starting solution.

Acknowledgment. J.X. acknowledges the Singapore–MIT Alliance program for his research scholarship.

Supporting Information Available: Figure S1, UV–vis and SDS–PAGE analyses of the algal extract; Figure S2, UV–vis spectra of Ag nanoparticles produced in L-Tyr and *O*-methyl-L-Tyr; Figure S3, FESEM images of Ag nanocrystals formed in different peptide solutions and the corresponding UV–vis spectra; and Table S1, summary of product morphology, product dimensions, SPR characteristics, and percentage conversions of Ag ions in different peptide solutions. This material is available free of charge *via* the Internet at http://pubs.acs.org.

REFERENCES AND NOTES

1 Raveendran, P.; Fu, J.; Wallen, S. L. Completely "Green" Synthesis and Stabilization of Metal Nanoparticles. *J. Am. Chem. Soc.* **2003**, *125*, 13940–13941.

2 Klaus, T.; Joerger, R.; Olsson, E.; Granqvist, C. G. Silver-based Crystalline Nanoparticles, Microbially Fabricated. *Proc. Natl. Acad. Sci. U.S.A.* **1999**, *96*, 13611–13614.

3 Nair, B.; Pradeep, T. Coalescence of Nanoclusters and Formation of Submicron Crystallites Assisted by *Lactobacillus* Strains. *Cryst. Growth Des.* **2002**, *2*, 293–298.

4 Ahmad, A.; Senapati, S.; Khan, M. I.; Kumar, R.; Ramani, R.; Srinivas, V.; Sastry, M. Intracellular Synthesis of Gold Nanoparticles by a Novel Alkalotolerant Actinomycete, *Rhodococcus* Species. *Nanotechnology* **2003**, *14*, 824–828.

5 Ahmad, A.; Senapati, S.; Khan, M. I.; Kumar, R.; Sastry, M. Extracellular Biosynthesis of Monodisperse Gold Nanoparticles by a Novel Extremophilic Actinomycete, *Thermomonospora* sp. *Langmuir* **2003**, *19*, 3550–3553.

6 Cunningham, D. P.; Lundie, L. L. Precipitation of Cadmium by Clostridium-Thermoaceticum. *Appl. Environ. Microbiol.* **1993**, *59*, 7–14.

7 Labrenz, M.; Druschel, G. K.; Thomsen-Ebert, T.; Gilbert, B.; Welch, S. A.; Kemner, K. M.; Logan, G. A.; Summons, R. E.; Stasio, G. D.; Bond, P. L.; *et al.* Formation of Sphalerite (ZnS) Deposits in Natural Biofilms of Sulfate-Reducing Bacteria. *Science* **2000**, *290*, 1744–1747.

8 Lovley, D. R.; Stolz, J. F.; Nord, G. L.; Phillips, E. J. P. Anaerobic Production of Magnetite by a Dissimilatory Iron-Reducing Microorganism. *Nature* **1987**, *330*, 252–254.

9 Kowshik, M.; Vogel, W.; Urban, J.; Kulkarni, S. K.; Paknikar, K. M. Microbial Synthesis of Semiconductor PbS Nanocrystallites. *Adv. Mater.* **2002**, *14*, 815–818.

10 Kowshik, M.; Deshmukh, N.; Vogel, W.; Urban, J.; Kulkarni, S. K; Paknikar, K. M. Microbial Synthesis of Semiconductor CdS Nanoparticles, Their Characterization, and Their Use in the Fabrication of an Ideal Diode. *Biotechnol. Bioeng.* **2002**, *78*, 583–588.

11 Kowshik, M.; Ashtaputre, S.; Kharrazi, S.; Vogel, W.; Urban, J.; Kulkarni, S. K.; Paknikar, K. M. Extracellular Synthesis of Silver Nanoparticles by a Silver-Tolerant Yeast Strain MKY3. *Nanotechnology* **2003**, *14*, 95–100.

12 Mukherjee, P.; Ahmad, A.; Mandal, D.; Senapati, S.; Sainkar, S. R.; Khan, M. I.; Parishcha, R.; Ajaykumar, P. V.; Alam, M.; Kumar, R.; Sastry, M. Fungus-Mediated Synthesis of Silver Nanoparticles and Their Immobilization in the Mycelial Matrix: A Novel Biological Approach to Nanoparticle Synthesis. *Nano Lett.* **2001**, *1*, 515–519.

13 Ahmad, A.; Mukherjee, P.; Senapati, S.; Mandal, D.; Khan, M. I.; Kumar, R.; Sastry, M. Extracellular Biosynthesis of Silver Nanoparticles Using the Fungus *Fusarium oxysporum*. *Colloids Surf. B* **2003**, *28*, 313–318.

14 Mukherjee, P.; Ahmad, A.; Mandal, D.; Senapati, S.; Sainkar, S. R.; Khan, M. I.; Ramani, R.; Parischa, R.; Ajayakumar, P. V.; Alam, M.; et al. Bioreduction of $AuCl_4^-$ Ions by the Fungus, *Verticillium sp.* and Surface Trapping of the Gold Nanoparticles Formed. *Angew. Chem., Int. Ed.* **2001**, *40*, 3585–3588.

15 Nie, S.; Emory, S. R. Probing Single Molecules and Single Nanoparticles by Surface-Enhanced Raman Scattering. *Science* **1997**, *275*, 1102–1106.

16 Velve, O. D.; Kaler, E. W. In Situ Assembly of Colloidal Particles into Miniaturized Biosensors. *Langmuir* **1999**, *15*, 3693–3698.

17 Nicewarner-Pena, S. R.; Freeman, R. G.; Reiss, B. D.; He, L.; Pena, D. J.; Walton, I. D.; Cromer, R.; Keating, C. D.; Natan, M. J. Submicrometer Metallic Barcodes. *Science* **2001**, *294*, 137–141.

18 Wiley, B.; Sun, Y.; Mayers, B.; Xia, Y. Shape-Controlled Synthesis of Metal Nanostructures: The Case of Silver. *Chem. Eur. J.* **2005**, *11*, 454–463.

19 Lee, K. S.; El-Sayed, M. A. Gold and Silver Nanoparticles in Sensing and Imaging: Sensitivity of Plasmon Response to Size, Shape, and Metal Composition. *J. Phys. Chem. B* **2006**, *110*, 19220–19225.

20 Sun, R. W. Y.; Chen, R.; Chung, N. P. Y.; Ho, C. M.; Lin, C. L. S.; Che, C. M. Silver Nanoparticles Fabricated in Hepes Buffer Exhibit Cytoprotective Activities toward HIV-1 Infected Cells. *Chem. Commun.* **2005**, 5059–5061.

21 Wright, J. B.; Lam, K.; Hansen, D.; Burrell, R. E. Efficacy of Topical Silver Against Fungal Burn Wound Pathogens. *Am. J. Infect. Control.* **1999**, *27*, 344–350.

22 Shankar, S. S.; Rai, A.; Ahmad, A.; Sastry, M. Rapid Synthesis of Au, Ag, and Bimetallic Au Core-Ag Shell

Nanoparticles Using Neem (*Azadirachta indica*) Leaf Broth. *J. Colloid Interface Sci.* **2004**, *275*, 496–502.
23 Shankar, S. S.; Ahmad, A.; Sastry, M. Geranium Leaf Assisted Biosynthesis of Silver Nanoparticles. *Biotechnol. Prog.* **2003**, *19*, 1627–1631.
24 Xie, J.; Lee, J. Y.; Wang, D. I. C.; Ting, Y. P. Identification of Active Biomolecules in the High-Yield Synthesis of Single-Crystalline Gold Nanoplates in Algal Solutions. *Small* **2007**, *3*, 672–682.
25 Jin, R.; Cao, Y. C.; Hao, E.; Metraux, G. S.; Schatz, G. C.; Mirkin, C. A. Controlling Anisotropic Nanoparticle Growth through Plasmon Excitation. *Nature* **2003**, *425*, 487–490.
26 Sun, Y.; Xia, Y. Triangular Nanoplates of Silver: Synthesis, Characterization, and Use as Sacrificial Templates For Generating Triangular Nanorings of Gold. *Adv. Mater.* **2003**, *15*, 695–699.
27 Sun, Y.; Mayers, B.; Xia, Y. Transformation of Silver Nanospheres into Nanobelts and Triangular Nanoplates through a Thermal Process. *Nano Lett.* **2003**, *3*, 675–679.
28 Bastys, V.; Pastoriza-Santos, I.; Rodriguez-Gonzalez, B.; Vaisnoras, R.; Liz-Marzan, L. M. Formation of Silver Nanoprisms with Surface Plasmons at Communication Wavelengths. *Adv. Funct. Mater.* **2006**, *16*, 766–773.
29 Metraux, G. S.; Mirkin, C. A. Rapid Thermal Synthesis of Silver Nanoprisms with Chemically Tailorable Thickness. *Adv. Mater.* **2005**, *17*, 412–415.
30 Chen, S.; Fan, Z.; Carroll, D. L. Silver Nanodisks: Synthesis, Characterization, and Self-Assembly. *J. Phys. Chem. B* **2002**, *106*, 10777–10781.
31 Maillard, M.; Giorgio, S.; Pileni, M. P. Silver Nanodisks. *Adv. Mater.* **2002**, *14*, 1084–1086.
32 Pastoriza-Santos, I.; Liz-Marzan, L. M. Synthesis of Silver Nanoprisms in DMF. *Nano Lett.* **2002**, *2*, 903–905.
33 Burda, C.; Chen, X.; Narayanan, R.; El-Sayed, M. A. Chemistry and Properties of Nanocrystals of Different Shapes. *Chem. Rev.* **2005**, *105*, 1025–1102.
34 Liz-Marzan, L. M. Tailoring Surface Plasmons through the Morphology and Assembly of Metal Nanoparticles. *Langmuir* **2006**, *22*, 32–41.
35 Tao, A.; Sinsermsuksakul, P.; Yang, P. Polyhedral Silver Nanocrystals with Distinct Scattering Signatures. *Angew. Chem., Int. Ed.* **2006**, *45*, 4597–4601.
36 Kirkland, A. I.; Jefferson, D. A.; Duff, D. G.; Edwards, P. P.; Gameson, I.; Johnson, B. F. G.; Smith, D. J. Structural Studies of Trigonal Lamellar Particles of Gold and Silver. *Proc. R. Soc. London Ser. A* **1993**, *440*, 589–609.
37 Germain, V.; Li, J.; Ingert, D.; Wang, Z. L.; Pileni, M. P. Stacking Faults in Formation of Silver Nanodisks. *J. Phys. Chem. B* **2003**, *107*, 8717–8720.
38 Rodriguez-Gonzalez, B.; Pastoriza-Santos, I.; Liz-Marzan, L. M. Bending Contours in Silver Nanoprisms. *J. Phys. Chem. B* **2006**, *110*, 11796–11799.
39 Wiley, B.; Herricks, T.; Sun, Y.; Xia, Y. Polyol Synthesis of Silver Nanoparticles: Use of Chloride and Oxygen to Promote the Formation of Single-Crystal, Truncated Cubes and Tetrahedrons. *Nano Lett.* **2004**, *4*, 1733–1739.
40 Xiong, Y.; Chen, J.; Wiley, B.; Xia, Y. Understanding the Role of Oxidative Etching in the Polyol Synthesis of Pd Nanoparticles with Uniform Shape and Size. *J. Am. Chem. Soc.* **2005**, *127*, 7332–7333.
41 Xia, Y.; Yang, P.; Sun, Y.; Wu, Y.; Mayers, B.; Gates, B.; Yin, Y.; Kim, F.; Yan, H. One-Dimensional Nanostructures: Synthesis, Characterization, and Applications. *Adv. Mater.* **2003**, *15*, 353–389.
42 Ignatenko, A. V.; Cherenkevich, S. N.; Komyak, A. I. Chromatographic and Spectroscopic Investigation of the Products of Oxidation of Tyrosine with Ozone. *J. Appl. Spectrosc.* **1984**, *41*, 798–802.
43 Riordan, J. F.; Wacker, W. E. C.; Vallee, B. L. *N*-Acetylimidazole: A Reagent for Determination of "Free" Tyrosyl Residues of Proteins. *Biochemistry* **1965**, *4*, 1758–1765.
44 Riordan, J. F.; Wacker, W. E. C.; Vallee, B. L. "Buried" Tyrosyl Residues and the Activity of Trypsin. *Nature* **1965**, *208*, 1209–1211.
45 Riordan, J. F.; Vallee, B. L. Acetylation. *Methods Enzymol.* **1972**, *25B*, 494–506.
46 Coates, J. Interpretation of Infrared Spectra, A Practical Approach. In *Encyclopedia of Analytical Chemistry*; Meyers, R. A., Ed.; John Wiley & Sons Ltd.: Chichester, 2000.
47 Lopez-Gallego, F.; Montes, T.; Fuentes, M.; Alonso, N.; Grazu, V.; Betancor, L.; Guisan, J. M.; Fernandez-Lafuente, R. Improved Stabilization of Chemically Aminated Enzymes via Multipoint Covalent Attachment on Glyoxyl Supports. *J. Biotechnol.* **2005**, *116*, 1–10.
48 Naik, R. R.; Stringer, S. J.; Agarwal, G.; Jones, S. E.; Stone, M. O. Biomimetic Synthesis and Patterning of Silver Nanoparticles. *Nat. Mater.* **2002**, *1*, 169–172.
49 Yu, L.; Banerjee, I. A.; Matsui, H. Direct Growth of Shape-Controlled Nanocrystals on Nanotubes via Biological Recognition. *J. Am. Chem. Soc.* **2003**, *125*, 14837–14840.
50 Sjodin, M.; Styring, S.; Akermark, B.; Sun, L.; Hammarstrom, L. Proton-Coupled Electron Transfer from Tyrosine in a Tyrosine-Ruthenium-tris-Bipyridine Complex: Comparison with Tyrosine$_Z$ Oxidation in Photosystem II. *J. Am. Chem. Soc.* **2000**, *122*, 3932–3936.
51 Merril, C. R.; Harrington, M.; Alley, V. A Photodevelopment Silver Stain for the Rapid Visualization of Proteins Separated on Polyacrylamide Gels. *Electrophoresis* **1984**, *5*, 289–297.
52 Rabilloud, T. Mechanisms of Protein Silver Staining in Polyacrylamide Gels—A 10-Year Synthesis. *Electrophoresis* **1990**, *11*, 785–794.
53 *CRC Handbook of Chemistry and Physics*, 87th ed.; Electronic version via Chapman & Hall/CRC Press, 2006–2007.
54 Pillai, Z. S.; Kamat, P. V. What Factors Control the Size and Shape of Silver Nanoparticles in the Citrate Ion Reduction Method? *J. Phys. Chem. B* **2004**, *108*, 945–951.
55 Chu, H. C.; Kuo, C. H.; Huang, M. H. Thermal Aqueous Solution Approach for the Synthesis of Triangular and Hexagonal Gold Nanoplates with Three Different Size Ranges. *Inorg. Chem.* **2006**, *45*, 808–813.
56 Zhang, F.; Gao, J.; Weng, J.; Tan, C.; Ruan, K.; Xu, C.; Jiang, D. Structural and Functional Differentiation of Three Groups of Tyrosine Residues by Acetylation of *N*-Acetylimidazole in Manganese Stabilizing Protein. *Biochemistry* **2005**, *44*, 719–725.